

Toward autonomous large eddy simulations of turbulence based on interscale energy transfer among resolved scales

J. Andrzej Domaradzki *

*Department of Aerospace and Mechanical Engineering, University of Southern California,
Los Angeles, California 90089-1191, USA*



(Received 10 June 2021; accepted 4 October 2021; published 20 October 2021)

In the present work we show how the subgrid-scale (SGS) energy transfer among resolved scales in large eddy simulations (LESs) and its wave number distribution can be obtained from the evolving LES velocity fields. This information, supplemented by the known asymptotic properties of energy flux in the inertial range, when cast in the form of a spectral eddy viscosity, allows self-contained simulations without use of extraneous SGS models. The method is tested in LESs of isotropic turbulence at high Reynolds number where the inertial range dynamics is expected and for lower-Reynolds-number decaying turbulence under conditions of the classical Comte-Bellot–Corrsin experiments.

DOI: [10.1103/PhysRevFluids.6.104606](https://doi.org/10.1103/PhysRevFluids.6.104606)

I. INTRODUCTION

The large eddy simulation (LES) equations for an incompressible flow are obtained by applying a filtering operation to the Navier-Stokes equations

$$\frac{\partial}{\partial t} \bar{u}_i + \frac{\partial}{\partial x_j} \bar{u}_i \bar{u}_j = -\frac{1}{\rho} \frac{\partial}{\partial x_i} \bar{p} + \nu \frac{\partial^2}{\partial x_j \partial x_j} \bar{u}_i - \frac{\partial}{\partial x_j} \tau_{ij}, \quad (1)$$

$$\frac{\partial}{\partial x_i} \bar{u}_i = 0, \quad (2)$$

where $u_i = (u_1, u_2, u_3) = (u, v, w)$, p , and ν are the velocity, pressure, and kinematic viscosity, respectively, and τ_{ij} is the subgrid-scale (SGS) stress tensor

$$\tau_{ij} = \bar{u}_i \bar{u}_j - \bar{u}_i \bar{u}_j. \quad (3)$$

The LES equations have the form of the Navier-Stokes equations for the filtered velocity \bar{u}_i plus the additional force term which is the divergence of the subgrid-scale stress tensor (3) and which is required to close the LES equations. Large eddy simulation procedures differ in how the SGS stress tensor is expressed (or modeled) in terms of the filtered velocity \bar{u}_i , but all SGS models aspire to the same goal. That goal is to obtain flow quantities for resolved scales as close as possible to those that would be obtained from filtered results of fully resolved DNS, if such DNS could be performed. Note that the meaning of “as close as possible” can be made more precise by using a method developed by Toosi and Larsson [1] to compute a relative error between LES results and direct numerical simulation (DNS) benchmarks. In constructing SGS models a large number of different approaches have been tried (see reviews and monographs [2–9]) but no clear consensus on the best SGS model or the best route to develop better models has been reached. This is partially because there are more pressing practical needs for modeling wall bounded flows in complex geometries, wall modeling for high-Reynolds-number or high-Mach-number incompressible or compressible

*jad@usc.edu

flows, and models accounting for additional physical phenomena such as heat transfer and chemical reactions. Each of those phenomena presents a different modeling challenge and a unified modeling framework may not exist. Another factor may be that common SGS modeling approaches rely on physical analogies (between eddy viscosity and molecular viscosity), mathematical identities (the dynamic procedure), or properties of discretization errors (implicit LES), which may not be sufficient to fully capture the physics of nonlinear interactions in turbulence responsible for SGS processes. Because of that we believe that it is beneficial to consider modeling approaches that explicitly account for physical properties of interscale interactions deduced from theory and observed in numerical simulations of turbulent flows. Such an approach to SGS modeling was introduced by Kraichnan [10] and developed further by Chollet and Lesieur [11]. In both cases two different analytical theories of turbulence [the test field model (TFM) and eddy damped quasinormal Markovian (EDQNM) approximation] were used to compute the SGS energy transfer. The computed SGS transfer is then normalized to cast it in a form of a wave-number-dependent eddy viscosity which can be used directly in LES. A good overview of these approaches can be found in [8,12]. More recently, a similar approach to SGS modeling has been proposed by Domaradzki [13], the main difference being that the total SGS transfer is computed not from analytical theories but from LES velocity fields being advanced in the simulations. The method was implemented in LES of high-Reynolds-number isotropic turbulence and evaluated for several classical spectral eddy viscosity models, with the total SGS transfer serving as a constraint for models. It was shown that the performance of models depends on their ability to capture not only the total SGS dissipation (which is enforced by the method) but also the distribution of the SGS dissipation among scales of motion (which is enforced by a model). In the present paper we show that in addition to the total SGS transfer it is also possible to extract the wave-number dependence of the spectral eddy viscosity from evolving LES fields, allowing for nearly autonomous LESs. An ideal, fully autonomous LES can be defined as a simulation that produces the same quality results within a resolved range of scales like DNS and uses only the same information that is available to DNS. In other words, in the ideal case the inputs (geometry of a domain, initial and boundary conditions, and the value of the kinematic viscosity) to and outputs from LES and DNS (physical quantities in the resolved range) are the same, the only difference being numerical resolution in DNS and LES. Because of the chaotic nature of turbulence comparisons between DNS and LES, results should be understood as comparisons between statistically averaged quantities. In the present work we cannot claim a fully autonomous LES because we rely also on the asymptotic behavior of energy flux in isotropic turbulence as an input, which would not be needed in fully resolved DNS. However, the properties of the energy flux for isotropic turbulence are well known from theoretical and DNS investigations [6,12,14–16]. Since they are well established and noncontroversial we feel that it is justified to call the presented approach a nearly or semiautonomous LES. The fundamental strength of this approach is that it is based on the physics of interscale energy transfers in turbulence, offering a major advantage over models relying primarily on phenomenological considerations.

II. SGS MODELING PROCEDURE AND NUMERICAL METHODS

In this section we provide a summary description of the SGS modeling approach and numerical methods used in this research which are elaborated on in more detail in the recent paper [13].

For testing the proposed procedure we choose isotropic, homogeneous turbulence simulated using pseudospectral Fourier methods. The flow is assumed to be contained in a cube of side $L = 2\pi$ and periodic boundary conditions in all three spatial directions are imposed on the independent variables. The domain is discretized in physical space using N uniformly spaced grid points in each direction resulting in a mesh size $\Delta x = L/N$ and a total of N^3 grid points. The independent variables are transformed between physical and spectral space using the discrete Fourier transform

$$\mathbf{u}(\mathbf{k}) = \frac{1}{N^3} \sum_{\mathbf{x}} \mathbf{u}(\mathbf{x}) \exp(-i\mathbf{k} \cdot \mathbf{x}) \quad (4)$$

and the inverse transform

$$\mathbf{u}(\mathbf{x}) = \sum_{\mathbf{k}} \mathbf{u}(\mathbf{k}) \exp(i\mathbf{k} \cdot \mathbf{x}), \quad (5)$$

where \mathbf{x} are the mesh points in physical space and \mathbf{k} are the discrete wave numbers with components $k_i = \pm n_i \Delta k$, with $n_i = 0, 1, 2, \dots, N/2$; $i = 1, 2, 3$; and $\Delta k = 2\pi/L = 1$. The distinction between the physical and spectral representations for a given quantity is made through its argument \mathbf{x} or \mathbf{k} , respectively.

Navier-Stokes equations [Eqs. (1) and (2) with the SGS term neglected] can be transformed into spectral (Fourier) space (see, e.g., [6,12])

$$ik_n u_n(\mathbf{k}, t) = 0, \quad (6)$$

$$\left(\frac{\partial}{\partial t} + \nu k^2 \right) u_n(\mathbf{k}, t) = N_n(\mathbf{k}, t) - ik_n p(\mathbf{k}, t), \quad (7)$$

where the wave numbers \mathbf{k} are associated with the scales of turbulent motions and N_n is the Fourier transform of the nonlinear term

$$N_n(\mathbf{k}, t) = -ik_j \int d\mathbf{p} u_j(\mathbf{p}, t) u_n(\mathbf{k} - \mathbf{p}, t). \quad (8)$$

The equation for the energy amplitudes $\frac{1}{2}|u(\mathbf{k}, t)|^2 = \frac{1}{2}u_n(\mathbf{k}, t)u_n^*(\mathbf{k}, t)$, where the asterisk denotes a complex conjugate, follows from (7),

$$\frac{\partial}{\partial t} \frac{1}{2}|u(\mathbf{k}, t)|^2 = -2\nu k^2 \frac{1}{2}|u(\mathbf{k}, t)|^2 + T(\mathbf{k}, t), \quad (9)$$

where $T(\mathbf{k}, t)$ is the nonlinear energy transfer

$$T(\mathbf{k}, t) = \text{Re}[u_n^*(\mathbf{k})N_n(\mathbf{k}, t)]. \quad (10)$$

Physical quantities of interest for isotropic turbulence are described in terms of the scalar wave number $k = |\mathbf{k}|$ by averaging over thin spherical shells, e.g., the energy spectrum is defined as

$$E(k, t) = 4\pi k^2 \langle \frac{1}{2}u_n(\mathbf{k}, t)u_n^*(\mathbf{k}, t) \rangle, \quad (11)$$

where $\langle \dots \rangle$ denotes averaging over all modes in a shell of thickness Δk centered at $k = |\mathbf{k}|$. Similarly, shell averaged $T(\mathbf{k}, t)$ provides the classical energy transfer $T(k, t)$ in the spectral energy equation

$$\frac{\partial}{\partial t} E(k, t) = -2\nu k^2 E(k, t) + T(k, t), \quad (12)$$

where the first term on the right-hand side is a viscous dissipation spectrum

$$D(k, t) = 2\nu k^2 E(k, t). \quad (13)$$

For brevity, in subsequent formulas, explicit time dependence will be omitted.

The equations are solved using a pseudospectral numerical method of Rogallo [17] in the implementation of Yeung and Pope [18]. For steady-state cases we use the forcing scheme of Sullivan *et al.* [19] in which the sum of squared amplitudes of velocity modes in a sphere of radius $K_f = 3.5\Delta k$ is kept constant in time. This is accomplished by multiplying all modes in the forced sphere by the same constant factor at the end of each time step to restore the energy in the sphere to the value at the beginning of the time step.

A number of turbulence parameters can be obtained from spectral quantities. The integral of $E(k)$ over k gives the turbulent kinetic energy per unit mass $\frac{3}{2}u'^2$, where u' is the rms turbulent velocity. The integrated dissipation spectrum gives the dissipation rate of the turbulent kinetic energy ε . The Taylor microscale is computed as $\lambda = (15u'^2\nu/\varepsilon)^{1/2}$ and the microscale Reynolds number is $\text{Re}_\lambda =$

$u'\lambda/\nu$. A timescale for the evolution of turbulence is the large eddy turnover time $T_e = L_{\text{int}}/u'$, where L_{int} is the integral length scale

$$L_{\text{int}} = \frac{\pi}{2u'^2} \int_0^\infty k^{-1} E(k) dk. \quad (14)$$

The macroscale Reynolds number is defined as $\text{Re} = u' L_{\text{int}}/\nu$.

Large eddy simulation techniques motivate interest in other quantities related to the nonlinear energy transfer $T(k)$. In spectral LES it is easy and natural to use a spherical, sharp spectral filter defined by a cutoff wave number k_c , separating resolved and subgrid scales. The spectral energy equation for resolved scales $\mathcal{E}(k_c) \equiv \int_0^{k_c} E(k) dk$ is

$$\frac{\partial}{\partial t} \mathcal{E}(k_c) \equiv \dot{\mathcal{E}}(k_c) = -2\nu \int_0^{k_c} k^2 E(k) dk + \Pi(k_c), \quad (15)$$

where the classical energy flux

$$\Pi(k_c) = \int_0^{k_c} T(k) dk \quad (16)$$

provides the energy transfer rate from all resolved scales (below k_c) to subgrid scales (above k_c).

The spectral LES energy equation for scales $k \leq k_c$ is obtained by defining first the energy transfer $T^<(k|k_c)$ among resolved modes, where the notation signifies that only modes satisfying the inequality $k \leq k_c$, i.e., scales that are fully known in LES with the cutoff k_c , are retained in computing $T^<(k|k_c)$. The complete spectral energy equation (12) can then be rewritten for LES scales $k \leq k_c$ as

$$\frac{\partial}{\partial t} E^<(k|k_c) = T^<(k|k_c) + T_{\text{SGS}}(k|k_c) - 2\nu k^2 E^<(k|k_c), \quad k \leq k_c, \quad (17)$$

where the SGS energy transfer term is

$$T_{\text{SGS}}(k|k_c) = T(k) - T^<(k|k_c), \quad k \leq k_c. \quad (18)$$

Note that $T(k)$ is the full nonlinear transfer from Eq. (12). Even though its values only in the resolved range $k \leq k_c$ are needed in Eq. (17), it is computed using all modes, resolved and subgrid scale.

Integrating Eq. (17) over resolved wave numbers gives Eq. (15) for $\mathcal{E}(k_c)$. Because nonlinear interactions among any subset of modes obtained using sharp spectral filters are energy conserving, the term $\int_0^{k_c} T^<(k|k_c) dk$ vanishes and the SGS energy transfer integrated over its wave-number domain, the so-called total SGS dissipation, satisfies the condition

$$\epsilon_{\text{SGS}}(k_c) \equiv T_{\text{SGS}}(k_c) = \int_0^{k_c} T_{\text{SGS}}(k|k_c) dk = \Pi(k_c). \quad (19)$$

Note that negative values of $T(k)$ signify energy losses at wave numbers k but traditionally the energy flux Π , the SGS energy transfer T_{SGS} , and the SGS dissipation ϵ_{SGS} are chosen to be positive if the resolved scales experience energy loss. For consistency with $T(k)$, we are not adopting this latter convention. When positive values of these quantities are needed we will use absolute values.

Following Kraichnan [10], the SGS spectral energy equation can be formally rewritten as

$$\frac{\partial}{\partial t} E^<(k|k_c) = T^<(k|k_c) - 2\nu_{\text{eddy}}(k|k_c) k^2 E^<(k|k_c) - 2\nu k^2 E^<(k|k_c), \quad (20)$$

where the SGS energy transfer is expressed in the same functional form as the molecular dissipation term by introducing the theoretical effective eddy viscosity

$$\nu_{\text{eddy}}(k|k_c) = -\frac{T_{\text{SGS}}(k|k_c)}{2k^2 E^<(k|k_c)}. \quad (21)$$

It should be stressed that the primary physical quantity is the energy transfer across a wave-number cutoff k_c between resolved scales ($k < k_c$) and subgrid scales ($k > k_c$) and the eddy viscosity is a derived quantity.

It was shown in [13] that the task of modeling $T_{\text{SGS}}(k|k_c)$ can be productively split into finding the total SGS transfer or dissipation (19) and separately its distribution in wave numbers k . The total SGS energy transfer across the cutoff k_c is determined by the formula, derived in [13],

$$T_{\text{SGS}}(k_c) = \frac{1}{1-b} T_{\text{SGS}}^{\text{res}}\left(\frac{1}{2}k_c\right), \quad (22)$$

where b is a constant and $T_{\text{SGS}}^{\text{res}}(\frac{1}{2}k_c)$ is the energy transfer computed for the resolved LES modes ($k < k_c$) and the cutoff $\frac{1}{2}k_c$. The expression (22) is obtained using the Germano identity and the assumption of the infinite inertial range. The Germano identity for SGS energy transfers, integrated over $k < \frac{1}{2}k_c$, is

$$T_{\text{SGS}}(\frac{1}{2}k_c) - \int_0^{(1/2)k_c} dk T_{\text{SGS}}(k|k_c) = T_{\text{SGS}}^{\text{res}}(\frac{1}{2}k_c). \quad (23)$$

Note that integrated SGS transfer terms are indicated by a dependence only on the cutoff wave number but not on k . For instance, the total resolved SGS transfer $T_{\text{SGS}}^{\text{res}}(\frac{1}{2}k_c)$ is found by first computing k -dependent SGS transfer using the expression (18),

$$T_{\text{SGS}}^{\text{res}}(k|\frac{1}{2}k_c) = T(k)^{<}(k|k_c) - T^{<}(k|\frac{1}{2}k_c), \quad k \leq \frac{1}{2}k_c, \quad (24)$$

where $T(k)^{<}(k|k_c)$ is the energy transfer for all resolved modes $k < k_c$ and $T^{<}(k|\frac{1}{2}k_c)$ is the transfer computed using only modes $k < \frac{1}{2}k_c$. Subsequently, (24) is integrated over $0 < k < \frac{1}{2}k_c$,

$$T_{\text{SGS}}^{\text{res}}(\frac{1}{2}k_c) = \int_0^{(1/2)k_c} dk T_{\text{SGS}}^{\text{res}}(k|\frac{1}{2}k_c), \quad (25)$$

providing the total SGS transfer for resolved modes across wave number $\frac{1}{2}k_c$. By definition, the quantity (25) can be computed using only resolved modes, known in LES with a cutoff k_c . For the infinite inertial range the energy flux across the spectrum is constant, allowing us to replace the first term in (23) by $T_{\text{SGS}}(k_c)$. The second term is a fraction of the total transfer $T_{\text{SGS}}(k_c)$ because the integration interval covers only a fraction of a wave-number domain contributing to $T_{\text{SGS}}(k_c)$, formally

$$\int_0^{(1/2)k_c} dk T_{\text{SGS}}(k|k_c) = b T_{\text{SGS}}(k_c), \quad (26)$$

where b is a constant to be determined. The above substitutions lead directly to the equation (22) for $T_{\text{SGS}}(k_c)$. The constant b ,

$$b = \frac{\int_0^{(1/2)k_c} dk T_{\text{SGS}}(k|k_c)}{T_{\text{SGS}}(k_c)}, \quad (27)$$

was determined in [13] using scaling properties of the energy flux Π introduced by Kraichnan [20,21] and DNS data from [15,22] and was found to be in the range 0.33–0.40. Once the value of b is chosen the total SGS energy transfer (19) can be determined uniquely for a given velocity field using only resolved modes $k \leq k_c$. Note that changing the constant b in the predicted range changes the total SGS transfer by at most 10%.

The wave-number distribution of $T_{\text{SGS}}(k|k_c)$ in [13] was prescribed explicitly through several spectral shape functions $f_i(k|k_c)$ for the effective eddy viscosity (21). Specifically, the eddy viscosity for a shape function f_i implemented in actual LES is

$$\nu_{\text{eddy}}(k|k_c) = C_m f_i(k|k_c), \quad (28)$$

where C_m is a model constant. The simplest shape function is $f_0 = 1$, corresponding to a wave-number-independent eddy viscosity. Other expressions are obtained using formulas for $T_{\text{SGS}}(k|k_c)$ computed numerically from analytical theories, assuming an infinite inertial range spectrum $k^{-5/3}$ [10–12]. For instance, the effective eddy viscosity (21) obtained using the EDQNM approximation is well fitted by the expression given by Chollet [23],

$$v_{\text{eddy}}(k|k_c) = C_m(0.441 + 15.2e^{-3.03k_c/k}) \equiv C_m f_1(k|k_c), \quad (29)$$

where f_1 is a spectral model shape function. The model constant C_m is computed using a known total SGS energy transfer as an integral constraint

$$T_{\text{SGS}}(k_c) = \int_0^{k_c} dk T_{\text{SGS}}(k|k_c) = - \int_0^{k_c} dk v_{\text{eddy}}(k|k_c) 2k^2 E(k), \quad (30)$$

which gives

$$C_m = \frac{-T_{\text{SGS}}(k_c)}{\int_0^{k_c} f_i(k|k_c) 2k^2 E(k) dk}. \quad (31)$$

In (31) $T_{\text{SGS}}(k_c)$ is expressed in terms of SGS transfer among resolved scales $T_{\text{SGS}}^{\text{res}}(\frac{1}{2}k_c)$, computed at each time step in LES with the spectral eddy viscosity given by (28). Since $T_{\text{SGS}}(k_c)$ and $E(k)$ in general are time dependent, C_m is also a function of time $C_m(t)$. Note that once a shape function is prescribed, the remaining information needed to determine $v_{\text{eddy}}(k|k_c)$ is obtained from the ongoing LES. In summary, the modeling procedure comprises two ingredients: (i) determination of the total SGS transfer $T_{\text{SGS}}(k_c)$ from the resolved fields and (ii) prescription for a functional form of the spectral shape function for the eddy viscosity.

There are two main goals of the present work. In a previous paper on this topic [13] it was shown that a shape function could be computed from the resolved fields and that it was qualitatively similar to the shape function f_1 , exhibiting a cusp at the cutoff k_c and an approximate plateau at low wave numbers. Implementing such a numerical shape function led to preliminary but encouraging results in actual LESs for high-Reynolds-number turbulence. This implies that if a shape function can be derived from LESs themselves the entire procedure may become autonomous, with no dependence (or only minimal dependence) on information input extraneous to LES. The first goal of this work is to investigate in more detail the feasibility of such autonomous LES. The second goal is to address turbulence at lower Reynolds numbers where assumptions of the inertial range dynamics made in the model development are no longer applicable.

III. LES OF HIGH-REYNOLDS-NUMBER TURBULENCE

For LES of high-Reynolds-number flows we follow closely methodology used in [13]. The main difference lies in the implementation of the eddy viscosity shape function. Less important is increased numerical resolution, from 32^3 in [13] to 64^3 modes here, to reduce fluctuations in computed spectra at higher wave numbers, and adding decaying turbulence cases (in Ref. [13] only forced cases were considered).

The possibility of an autonomous LES was suggested by the investigation in [13] of a wave-number distribution of the resolved SGS energy transfer $T_{\text{SGS}}^{\text{res}}(k|\frac{1}{2}k_c)$ [see Eq. (24)]. This quantity, cast in the form of the k -dependent eddy viscosity (21), was computed from LES data and is shown in Fig. 1 as $f_{\text{LES}}(k|\frac{1}{2}k_c)$. Large eddy simulations have been performed using the theoretical eddy viscosity (29), which is also plotted in Fig. 1. Both curves are normalized by their peak values at the cutoff. The curve obtained from LES data exhibits qualitatively the same behavior as the theoretical eddy viscosity: an approximate plateau for lower k followed by a cusp as the cutoff wave number is approached. Quantitatively, however, the plateau values computed from LES data are not uniformly constant and can be a factor of 2 less than plateau values for the shape function used to generate those data. A likely explanation for this quantitative inconsistency is that in computing $T_{\text{SGS}}^{\text{res}}(k|\frac{1}{2}k_c)$

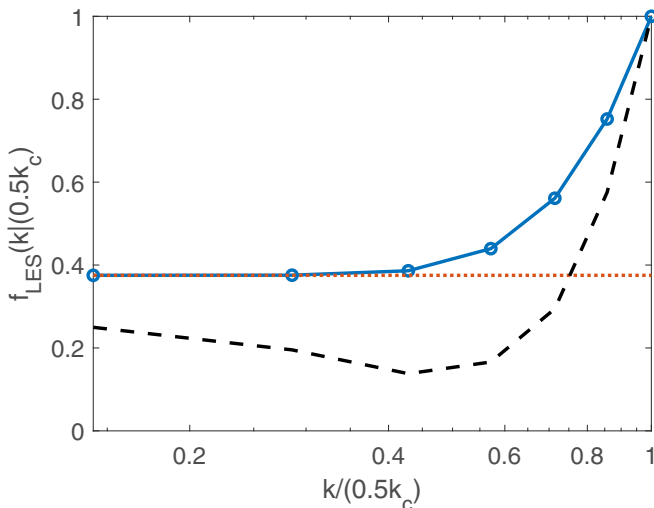


FIG. 1. Spectral eddy viscosity shape functions. The solid line with circles denotes the analytical expression (29), the dashed line shows a shape function computed from LES data, and the dotted line shows the asymptotic plateau value from the EDQNM theory

nonlinear interactions with unresolved scales $k > k_c$ are not accounted for, reducing the SGS energy transfer from the plateau range and thus the level of the eddy viscosity in that range. Nevertheless, the qualitative similarity of theoretical and computed spectral shape functions suggests that it should be possible to infer a shape function directly from LES, reducing the dependence of the method on information extraneous to actual simulations. In this work we propose a hybrid shape function that retains the cusp behavior obtained from LES data and replaces the computed plateau by an asymptotic eddy viscosity at $k \rightarrow 0$ obtained from theories of inertial range dynamics. In the asymptotic limit the ratio of the plateau value to the peak value at the cusp is $p = 0.37$, as obtained in [11,23] for the spectral eddy viscosity (29). That value is indicated by a horizontal line in Fig. 1. Operationally, the shape function is computed at each time step from LES data, resetting its values away from the cutoff to the asymptotic value of 0.37, rescaling from test cutoff $\frac{1}{2}k_c$ to LES cutoff k_c , and using the rescaled shape function in the next time step in LES. The rescaling is accomplished using the normalized wave number k/k_{cutoff} , i.e., in the present case

$$f_{\text{LES}}(k|k_c) = f_{\text{LES}}\left(\frac{k}{k_c}\right) = f_{\text{LES}}\left(k\left|\frac{1}{2}k_c\right.\right). \quad (32)$$

The proposed hybrid shape function is easy to implement and retains most of the information about the effects of the local energy transfers. For instance, the cusp in Fig. 1 between the asymptotic value at $k/k_{\text{cutoff}} \approx 0.75$ and the peak location at $k/k_{\text{cutoff}} = 1$ is responsible for about 50% of the total SGS transfer across the cutoff wave number. This local transfer is not modeled but is a result of the actual interscale interactions operating at a given time step in actual LES. The remainder of the SGS transfer is caused by more nonlocal interactions and is modeled by a k -independent eddy viscosity. A constant eddy viscosity acting at large scales is consistent with predictions of turbulence theories in the presence of scale separation.

The complete procedure is implemented in several steps. In all cases the velocity field is initialized in spectral space using the prescribed analytical form of the energy spectrum $E(k)$. From the relation (11) the velocity vector $u_n(\mathbf{k})$ has length $|u(\mathbf{k})| = \sqrt{E(k)/2\pi k^2}$. The velocity vector $u_n(\mathbf{k})$ for a given wave number \mathbf{k} is determined as a vector of this length normal to \mathbf{k} to enforce the incompressibility condition. The velocity direction in the plane normal to \mathbf{k} is random, obtained by

TABLE I. Simulated LES cases. In all cases the molecular viscosity is $\nu = 2.5 \times 10^{-7}$, the time step is $\Delta t = 0.005$, and the total simulation time is $T = 10$. Turbulence parameters are shown at the initial time for two different initial spectra (eKolm and ePulse) and at the final time for forced and decaying LES (suffix F and D, respectively).

Case	No. of steps	u'^2	ε	λ	Re_λ	T_e
eKolm initial time	1	1.105	0.5709	0.002 69	11 340	1.21
eKolmF	2000	1.232	0.5648	0.002 87	12 770	1.02
eKolmD	2000	0.082	0.0245	0.003 55	4070	2.67
ePulse initial time	1	2.293	1.2159	0.002 74	16 650	0.78
ePulseF	2000	2.260	1.2846	0.002 56	15 460	0.80
ePulseD	2000	0.087	0.0191	0.004 15	4890	3.28

selecting a phase angle for a two-dimensional vector in a plane from a random number generator. After the velocity is initialized the code advances velocity forward in time. Compared with the DNS code, for LESs the additional fractional step implements the modeling procedure. Specifically, the Navier-Stokes equation (7) is supplemented by the eddy viscosity term

$$\left(\frac{\partial}{\partial t} + \nu k^2\right)u_n(\mathbf{k}, t) = N_n(\mathbf{k}, t) - ik_n p(\mathbf{k}, t) - \nu_{\text{eddy}}(k, t)k^2 u_n(\mathbf{k}, t). \quad (33)$$

At each time step in simulations the eddy viscosity in Eq. (33) is computed as follows. First, the SGS transfer $T_{\text{SGS}}(k|\frac{1}{2}k_c)$ is computed from the velocity field in LES, where k_c is the LES cutoff and $\frac{1}{2}k_c$ is the test cutoff. Total SGS transfer $T_{\text{SGS}}(k_c)$ for the LES cutoff k_c is then computed using the formula (22) with $b = 0.4$. The eddy viscosity for the test cutoff is computed as

$$\nu_{\text{eddy}}(k|\frac{1}{2}k_c) = -\frac{T_{\text{SGS}}^{\text{res}}(k|\frac{1}{2}k_c)}{2k^2 E^<(k|\frac{1}{2}k_c)} \quad (34)$$

and normalized to unity at the test cutoff

$$f_{\text{LES}}(k|\frac{1}{2}k_c) = \frac{\nu_{\text{eddy}}(k|\frac{1}{2}k_c)}{\nu_{\text{eddy}}(\frac{1}{2}k_c|\frac{1}{2}k_c)}. \quad (35)$$

The normalized function $f_{\text{LES}}(k|\frac{1}{2}k_c)$ is then rescaled to the full LES cutoff k_c using the relation (32) and its values away from the cusp are replaced by the asymptotic value $p = 0.37$. This last step is equivalent to drawing a straight horizontal line in Fig. 1 and finding its intercept with the normalized eddy viscosity, say, at $k_i < k_c$. The final, hybrid shape function $f_{\text{LES}}(k|k_c)$ consists of the constant plateau $p = 0.37$ for $0 < k \leq k_i$ and a cusp for $k_i < k \leq k_c$, which is obtained directly from the actual SGS transfer in LES. Once the shape function is known, the eddy viscosity is obtained as $\nu_{\text{eddy}}(k|k_c) = C_m f_{\text{LES}}(k|k_c)$ [see Eq. (28)] with the coefficient C_m given by Eq. (31).

To test these concepts and the proposed method we have performed several forced and decaying large eddy simulations. More details about simulated cases are provided in Table I. Forcing is applied for modes with $k \leq 3.5$ by resetting at each time step the total energy in the forcing band to the value at the previous time step. The same forcing implementation was used for cases eKolmF and ePulseF. Some cases were initialized with the Kolmogorov spectral form $k^{-5/3}$, with no prefactors, and were run until a statistically steady state was reached. The simulations were continued in the steady state to collect statistics. The expectation is that a correct SGS model should maintain the $k^{-5/3}$ spectral form in a steady state with an appropriate value of the Kolmogorov constant. Also, forced turbulence spectra should tend asymptotically toward the Kolmogorov $k^{-5/3}$ form independently of the initial condition and SGS models should be able to capture this behavior. To test this expectation we have performed several LESs with a pulse-type initial condition where

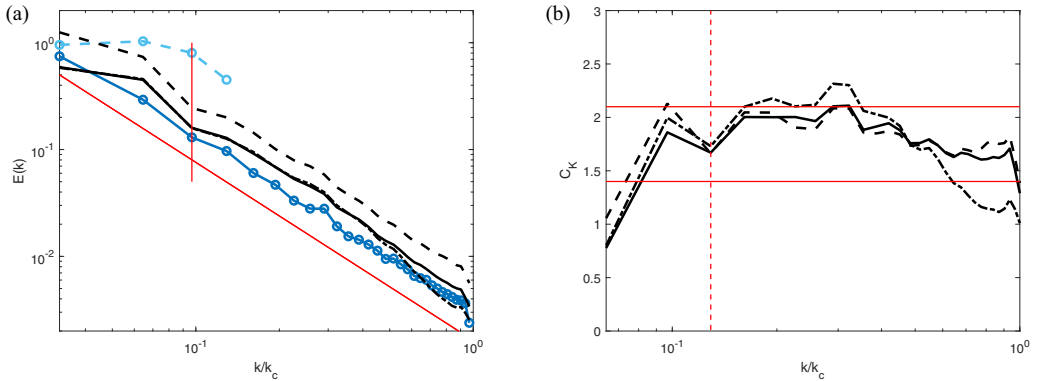


FIG. 2. Results for forced LES. (a) Lines with circles show the initial conditions for energy spectra. The solid line shows the case eKolmF, the dashed line the case ePulseF, and the dash-dotted line the results of LES performed with the Chollet-Lesieur spectral model. In this and all subsequent figures thin straight lines show, as appropriate, a $-5/3$ slope and a boundary of the forcing band at $k = 3$. (b) For compensated spectra horizontal lines mark the expected range of values for the Kolmogorov constant.

$E(k) = \text{const}$ for $k \leq 4$ and $E(k) = 0$ for $k > 4$. The secondary objective of this research is to minimize information input into LESs as compared with DNSs for the same physical problem. Obviously, the geometry, the initial and boundary conditions, and the kinematic viscosity can be easily matched. However, the initialization for LESs in principle should also include the eddy viscosity. One possibility is to start LESs with zero eddy viscosity and let it develop in the course of simulations. Another one is to prescribe an eddy viscosity shape function as a part of the initialization, as the kinematic viscosity is prescribed. We adopted the latter approach where, for a given initial velocity field, we run a short precursor no-model LES, i.e., DNS on a coarse LES grid, extract the numerical shape function at the end of such a run, and incorporate it as a part of an initialization for an actual LES. This procedure introduces some rudimentary information about an initial SGS energy transfer for a given field and at the same time is obtained entirely with information available from DNS. The length of the precursor run was from 10 to 50 time steps, with no special considerations to optimize it.

Note that turbulence parameters defined in Sec. II depend on the viscous dissipation ε which is dominated by the high-wave-number part of the energy spectrum, not available in LES. For high Reynolds numbers considered in this work the unknown viscous dissipation ε is assumed to be equal to the energy flux Π across the spectrum. In decaying LES we estimate Π through Eq. (15), as a difference between the energy decay rate for resolved scales and the known viscous dissipation in that range. In forced LES we estimate $\Pi = \varepsilon$ in a steady state as a difference between the measured energy input rate by forcing and the known viscous dissipation in the resolved range. The viscous dissipation in the resolved range was found to be four orders of the magnitude less than the estimated ε . Using this estimate, the initial Taylor microscale Reynolds number Re_λ in all cases exceeded 10^4 , confirming that the LESs considered are for high-Reynolds-number turbulence where the Kolmogorov theory should apply. The simulations were run for a minimum of 2000 time steps, with $\Delta t = 0.005$, which corresponds to about eight to twelve large eddy turnover times T_e , depending on the case, and the results were generally averaged over the last third of a runtime.

In Fig. 2 we plot the results of forced LESs for two different initializations: the $k^{-5/3}$ energy spectrum and a pulse energy spectrum. In both cases the spectral energy slopes at late times appear to be in excellent agreement with the $-5/3$ exponent. For the $k^{-5/3}$ initial condition we have performed also LES using the classical Chollet-Lesieur spectral model with the Kolmogorov constant $C_K = 1.4$. Its performance is respectable, but compared with two other cases the model is somewhat overly dissipative as the cutoff k_c is approached. The overall quality of predicted spectral slopes

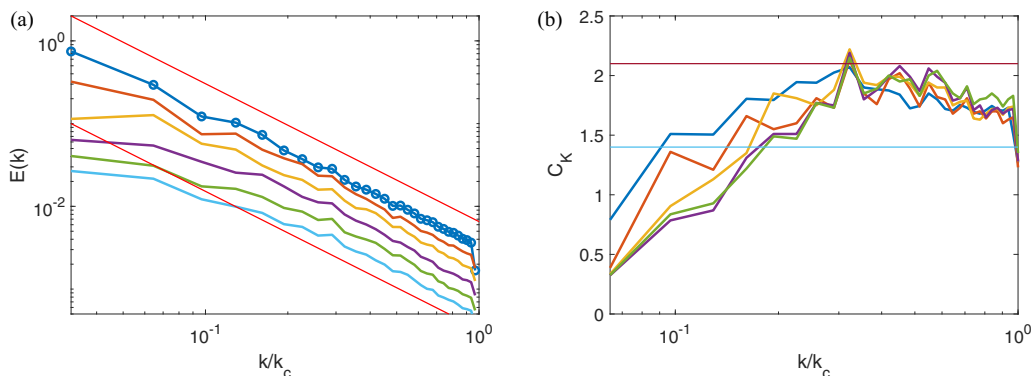


FIG. 3. Results for the decaying LES case eKolmD for (a) energy spectra and (b) compensated energy spectra. The line with circles denotes the initial condition and solid lines show energy spectra at different times of decay.

can be better evaluated by plotting compensated spectra in the form of a k -dependent Kolmogorov function

$$C_K(k) = \frac{E(k)}{\varepsilon^{2/3} k^{-5/3}}. \quad (36)$$

According to experimental and DNS investigations, $C_K(k)$ is expected to be a constant with a value in the range 1.4–2.1 for the perfect Kolmogorov range [24,25]. The function (36) is shown in Fig. 2(b) for all forced cases and models used. The values of $C_K(k)$ are not constant, especially within the forcing band, but fall within the expected range outside the forcing wave numbers. The overdissipation of the Chollet-Lesieur model close to the LES cutoff is reflected in values of C_K dropping below the expected range in that region. It is also worth noting that in SGS modeling sometimes model constants are determined assuming an inertial range with a particular value of the Kolmogorov constant (e.g., the standard Smagorinsky model or the Chollet-Lesieur spectral model considered here). For the method described in this paper the Kolmogorov constant, rather than being an input into the procedure, is one of its predictions.

In Figs. 3 and 4 we show results for LESs with the same initializations but without forcing. The total energy decreases during the decay to 7.5% and 3.8% of the initial value for cases eKolmD and

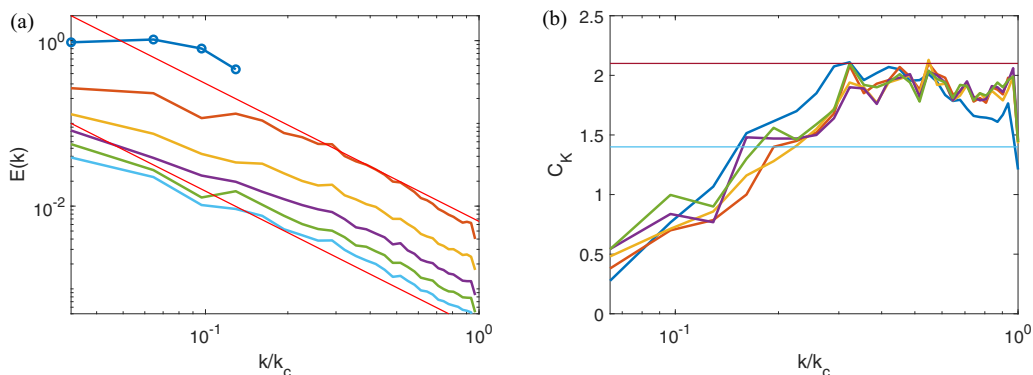


FIG. 4. Results for the decaying LES case ePulseD for (a) energy spectra and (b) compensated energy spectra. The line with circles denotes the initial condition and solid lines show energy spectra at different times of decay.

ePulseD, respectively. In both cases the energy spectra maintain the inertial range slope with correct values of the Kolmogorov constant C_K for wave numbers greater than $k \approx 8 = 0.27k_c$. For lower wave numbers slopes become progressively shallower, i.e., larger than $-5/3$, which is also reflected in values of C_K falling below the typical range. It is clear from the plots that the shallower spectra are the result of faster energy decay rates for low-wave-number modes than necessary to maintain the inertial range slope. This behavior can be explained by the fact that the energy spectrum ends at $k = 1$ and thus there is no energy flux from larger scales which would normally operate for an infinite inertial range and feed energy to low-wave-number modes in LES.

Overall, these results demonstrate that the performance of the proposed procedure in LES of high-Reynolds-number turbulence is quite good. Additionally, results are improved compared with the results shown in Ref. [13], which were obtained using prescribed functional forms for the eddy viscosity shape functions.

IV. LES OF LOW-REYNOLDS-NUMBER DECAYING TURBULENCE

The modeling approach developed above relies on asymptotic properties of the energy flux in the inertial range of high-Reynolds-number turbulence, implying values of constants $b \approx 0.4$ and $p \approx 0.37$, for both stationary and decaying flows. At lower Reynolds numbers, when the inertial range is not present, these assumptions are questionable. For instance, for a cutoff k_c in the vicinity of the dissipation range the energy transfer is dominated by local interactions and, additionally, viscous dissipation effects cannot be neglected in the kinetic energy balance used to determine the SGS energy transfer [15,22,26,27]. Under such physical conditions the spectral eddy viscosity is found to exhibit predominantly the cusp behavior at k_c and a negligible level of plateau away from k_c (see [8,12,28]). Additional complications are introduced for decaying turbulence because the fixed cutoff wave number k_c will drift further into the dissipative range as decay progresses, implying that constants b and p may be changing in time.

To assess the potential effect of these issues on the proposed SGS modeling we consider the spectral energy equation (15) for two cutoffs k_c and ak_c with $a < 1$, say, $a = \frac{1}{2}$. Subtracting these equations gives

$$\dot{\mathcal{E}}(k_c) - \dot{\mathcal{E}}(\frac{1}{2}k_c) \equiv \dot{\mathcal{E}}(\frac{1}{2}k_c < k < k_c) = -2\nu \int_{(1/2)k_c}^{k_c} k^2 E(k) dk + \Pi(k_c) - \Pi(\frac{1}{2}k_c), \quad (37)$$

which provides the equation for $\Pi(k_c)$,

$$|\Pi(k_c)| = |\Pi(\frac{1}{2}k_c)| + |\dot{\mathcal{E}}(\frac{1}{2}k_c < k < k_c)| - 2\nu \int_{(1/2)k_c}^{k_c} k^2 E(k) dk, \quad (38)$$

where the energy fluxes and the energy decay rate for the range $\frac{1}{2}k_c < k < k_c$ are explicitly written as positive terms. Note that for wave numbers $\frac{1}{2}k_c$ and k_c in the inertial range the energy decay rates in (37) are approximately equal (the decay rate is determined by much larger scales $k \ll k_c$) and the viscous dissipation term in (38) is approximately zero (the viscous dissipation is determined by much smaller scales $k \gg k_c$) so that $|\Pi(k_c)| \approx |\Pi(\frac{1}{2}k_c)|$. This well-known result for the constancy of the energy flux in the inertial range was used in Ref. [13] as one of the conditions to relate the total SGS transfer at k_c to the resolved SGS transfer at test cutoff $\frac{1}{2}k_c$. The second condition required in the procedure was the fraction b of the total transfer across k_c coming from the range $k < \frac{1}{2}k_c$, which was determined as $b \approx 0.4$ for the inertial range. In a steady state one effect on the flux at k_c is that, compared with the flux at $\frac{1}{2}k_c$, it is diminished by the amount of the viscous dissipation in the range $\frac{1}{2}k_c < k < k_c$. This is because the second term on the right-hand side of (38) vanishes in a steady state. The second effect is a diminished fraction b of the total SGS transfer from scales $k < \frac{1}{2}k_c$ if the cutoff is outside the inertial range. To assess these effects we have reanalyzed data from forced DNSs of isotropic turbulence performed with 512^3 resolution at $\text{Re}_\lambda \approx 200$ in our

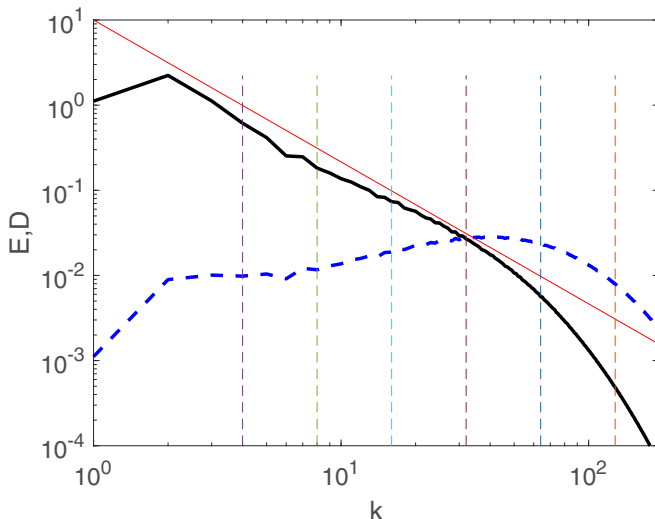


FIG. 5. Energy and dissipation spectra for forced DNSs. The solid line shows the energy spectrum and the dashed line shows the dissipation spectrum; dashed straight vertical lines denote wave-number band boundaries and the $-5/3$ slope is indicated by a straight solid line.

previous work [15,27]. The energy and viscous dissipation spectra from those DNSs are plotted in Fig. 5.

The wave-number domain is divided into spherical bands with band boundaries given in Table II and marked in Fig. 5 by vertical lines. In Table II column 2 shows the total viscous dissipation in a band between values of k_c in that row and the previous row (the first band is $0 < k < 4$). The next column gives the difference in the fluxes at the band boundaries, which is the energy input

TABLE II. Energy flux decomposition for wave-number bands. Column headings denote the following: k_c , band boundaries; Dissipation, viscous dissipation for a band between k_c in that row and the previous row; $|\Pi(\frac{1}{2}k_c)| - |\Pi(k_c)|$, energy flux into the band [see Eq. (38)]; $\Pi(k_c)$, the total energy flux at k_c ; columns with headings $k = 4, 8, \dots, 128$ give contributions to the total flux $\Pi(k_c)$ from bands with $k \leq k_c$, actual values and percentages of $\Pi(k_c)$; b , the parameter b computed from data in a row k_c using Eq. (27).

k_c	Dissipation	$ \Pi(\frac{1}{2}k_c) $ $- \Pi(k_c) $	$\Pi(k_c)$	4	8	16	32	64	128	b
4	0.0300	-2.6619	-2.6619	-2.6619						
				100%						
8	0.0433	-0.0589	-2.7208	-0.8883	-1.8325					0.33
				33%	67%					
16	0.1284	0.0727	-2.6481	-0.3465	-0.5858	-1.7158				0.35
				13%	22%	65%				
32	0.3907	0.4074	-2.2407	-0.0679	-0.1351	-0.3495	-1.6882			0.25
				3%	6%	16%	75%			
64	0.8553	0.8510	-1.3897	0.0038	-0.0024	-0.0191	-0.0693	-1.3026		0.06
				-0.3%	0.2%	1.4%	5%	94%		
128	0.9366	0.9596	-0.4301	0.0022	0.0030	0.0054	0.0120	0.0164	-0.4692	
				-0.5%	-0.7%	-1.3%	-2.8%	-3.8%	109%	
256	1.3207									

into the band due to nonlinear interactions. The total energy flux Π across k_c is provided in the next column, followed by decomposition of the flux into contributions from all bands below k_c for a given row. For instance, the row for $k_c = 16$ contains information about viscous dissipation in the band $8 \leq k \leq 16$ (0.1284), the total energy flux into the band (0.0727), the total flux across $k_c = 16$ (-2.6481), and contributions to the total flux from the bands $0 \leq k \leq 4$ (-0.3465), $4 \leq k \leq 8$ (-0.5858), and $8 \leq k \leq 16$ (-1.7158). The last column contains constant b computed from data in the table according to Eq. (27). Bands corresponding to $k_c = 8$ and 16 are firmly in the inertial range, away from the dissipation peak located between $k_c = 32$ and 64, and the equality $|\Pi(k_c)| = |\Pi(\frac{1}{2}k_c)|$ holds within 2–3 %. The constant b for these cutoffs is close to the value of 0.4 predicted by asymptotics. Inspection of values of Π and viscous dissipation in the table for $k_c \geq 32$ shows directly that the relation (38) is satisfied, i.e., the energy flux into the band is balanced by viscous dissipation [there are some minor discrepancies because the dissipation is computed from the energy spectrum as $2\nu k^2 E(k)$ rather than from averaging over individual wave-number modes in a shell $\langle |\mathbf{k}|^2 \frac{1}{2} u_n(\mathbf{k}, t) u_n^*(\mathbf{k}, t) \rangle$]. For the cutoff $k_c = 32$, just before the dissipation peak, the constant b decreases to 0.25, and for the cutoff $k_c = 64$, after the dissipation peak, the constant b becomes very small, indicating a preponderance of local energy transfers, i.e., 94% of the flux across $k_c = 64$ is from scales in the vicinity of the cutoff $\frac{1}{2}k_c \leq k \leq k_c$. This trend is consistent with the results of analytical theories of turbulence that show increasing contribution from local interactions for energy spectra with slopes steeper than the $-5/3$ inertial slope [3]. Additionally, for cutoff $k_c = 128$ in the dissipation range, negative contributions to the flux are observed for scales with wave numbers $k \leq \frac{1}{2}k_c$, indicating, albeit small, inverse energy transfer from the dissipative range to the energy containing range. Such inverse energy transfer has been documented previously in DNSs for low-Reynolds-number turbulence [26,28,29]. Based on this analysis, values of b smaller than 0.4 may be required for LESs of turbulence at low Reynolds numbers where the dynamics is dominated by dissipative rather than inertial effects.

Ultimately, the steady-state modeling for lower-Reynolds-number turbulence is not expected to be much different from the case of the inertial range modeling apart from the viscous modification of the flux relation (38) and possibly values of b lower than those for the inertial range dynamics. A more interesting case is freely decaying turbulence when all terms in Eq. (38) are nonzero. At low Reynolds numbers the energy peak, the dissipation peak, and the negative peak of the energy transfer term $T(k)$ are not widely separated and partially overlap [29]. The principal balance in the dissipation range $k\eta \geq 0.3$ is between the flux terms and the viscous dissipation term in Eq. (38), with $|\dot{\mathcal{E}}(\frac{1}{2}k_c < k < k_c)| \approx 0$, as in a steady state. However, in LESs of such flows the cutoff wave number k_c is normally located just outside the energy peak but before the dissipation peak, where the dissipation spectrum $-2\nu k^2 E(k)$ and the transfer spectrum $T(k)$ are of the same orders of magnitude and negative, contributing in tandem to rapid energy removal from the energy containing range. In that case the energy equation in LES with k_c , corresponding to the full energy equation (37), is

$$\dot{\mathcal{E}}(\frac{1}{2}k_c < k < k_c) = -2\nu \int_{(1/2)k_c}^{k_c} k^2 E(k) dk + \int_{(1/2)k_c}^{k_c} T_{\text{SGS}}(k|k_c) dk - T_{\text{SGS}}^{\text{res}}(\frac{1}{2}k_c). \quad (39)$$

Note that for decaying inertial range the viscous dissipation in this equation can be neglected and the energy decay rate for the range $\frac{1}{2}k_c < k < k_c$ is due to an imbalance between energy transfer to that range from scales $k < \frac{1}{2}k_c$ [given by $T_{\text{SGS}}^{\text{res}}(\frac{1}{2}k_c)$, known in LES] and the energy transfer from that range [given by the integral of modeled $T_{\text{SGS}}(k|k_c)$]. For the cutoff wave number k_c in the dissipation range none of the terms on the right-hand side of (39) can be neglected.

Despite these potential difficulties caused at low Reynolds numbers by the presence of viscous effects and increased complexity of the energy dynamics for decaying turbulence we found out, surprisingly, that the procedure, without any modifications, performs very well for an established test case. The test case is provided by the results of the classical experiments of Comte-Bellot and Corrsin [30] for decaying turbulence behind a grid in a wind tunnel. Among other results, the authors provided data for energy spectra measured at three times $tU_0/M = 42, 98, 171$, where

TABLE III. Comparison of turbulence parameters between LES and experiments [30]. The LES was performed with 64^3 resolution, initialized with the energy spectrum at $U_0 t/M = 42$ shown in Figs. 6 and 7. The parameters are defined as follows: u' , rms turbulent velocity; ε , dissipation rate; η , Kolmogorov microscale; λ , Taylor microscale; L_{int} , integral length scale; and R_λ , microscale Reynolds number. Experimental values are shown in parentheses, after conversion using a length unit $[L] = 0.1$ cm. In the first row the experimental data are at the initial time $\frac{U_0 t}{M} = 42$.

$\frac{U_0 t}{M}$	t (s)	u'	ε	η	λ	L_{int}	R_λ
51	0.213	1.93 (2.22)	17.7 (47.40)	0.0037 (0.0029)	0.0643 (0.0484)	0.34 (0.24)	82.7 (71.6)
98	0.498	1.24 (1.28)	5.61 (6.33)	0.0049 (0.0048)	0.0786 (0.0764)	0.40 (0.345)	65.0 (65.3)
171	0.868	0.894 (0.895)	1.85 (1.74)	0.0065 (0.0066)	0.099 (0.102)	0.46 (0.490)	59.0 (60.7)

$U_0 = 1000$ cm/s is a freestream velocity in the wind tunnel and $M = 5.08$ cm is the grid size. In numerical tests the velocity field is initialized to be consistent with the energy spectrum at $tU_0/M = 42$ and the task is to advance the fields in simulations and compare computed turbulence parameters and spectra with the experimental spectra at $tU_0/M = 98, 171$. The experimental results are provided in the dimensional form using cgs units, with the lowest reported wave number $k_e = 0.15$ cm $^{-1}$ and the highest $k_e = 20$ cm $^{-1}$ (the subscript e indicates experimental wave number). Since in pseudospectral numerical simulations the minimum wave number is by default equal to unity, the experimental data are converted into simulation data by changing the unit of length from centimeters to a new unit L : 1 cm = $k_e^{\text{min}} L$, where k_e^{min} is the numerical value of the minimum experimental wave number to be represented in the simulations. We extrapolated the Comte-Bellot–Corrsin data to the minimum wave number $k_e^{\text{min}} = 0.1$ cm $^{-1}$, with the maximum wave number kept at $k_e^{\text{max}} = 20$ cm $^{-1}$. In new units the simulation parameters are $\Delta k = 10\Delta k_e[L^{-1}] = 1[L^{-1}]$, $\nu = 0.1^2 \nu_e[L^2/s] = 0.0015[L^2/s]$ (for air, $\nu_e = 0.15$ cm $^2/s$), and the energy spectrum $E = 0.1^3 E_e[L^3/s^2]$ and time remains dimensional in seconds. All turbulent quantities can be converted in the same way for a comparison between simulation and experimental data. Some of such comparisons are collected in Table III.

In Fig. 6(a) we plot experimental energy and dissipation spectra from Comte-Bellot and Corrsin [30]. The thin vertical line indicates the cutoff wave number selected for simulations ($k_c = 30$, equivalent to $k_e = 3$ cm $^{-1}$ in cgs units). For all three time instants in the experiments the viscous dissipation peak is located outside the resolved range. Because the numerical resolution is unable

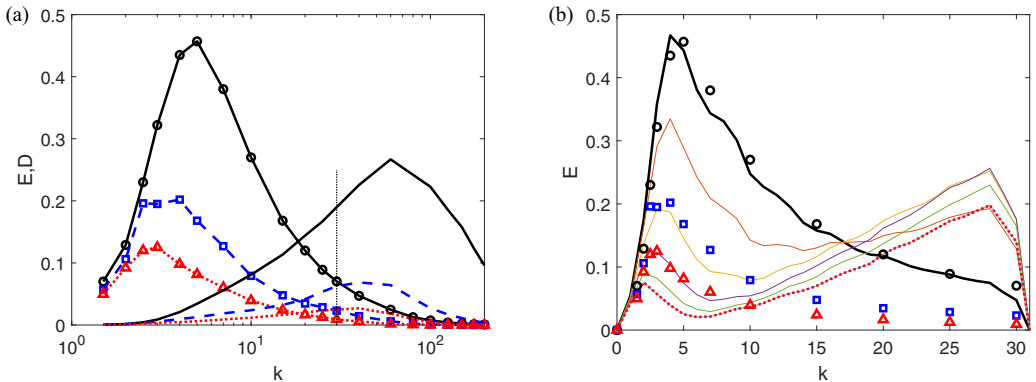


FIG. 6. (a) Experimental energy and viscous dissipation spectra at different times. Lines of the same type show energy spectra $E(k)$ (with symbols) and dissipation spectra $D(k)$ (without symbols): solid lines and circles, $U_0 t/M = 42$; dashed lines and squares, $U_0 t/M = 98$; and dotted lines and triangles, $U_0 t/M = 171$. (b) Time evolution of energy spectra in underresolved DNS. Markers correspond to experimental data and lines show progression in time from the initial energy spectrum at $U_0 t/M = 42$ to the final time at $U_0 t/M = 171$ (dotted line).

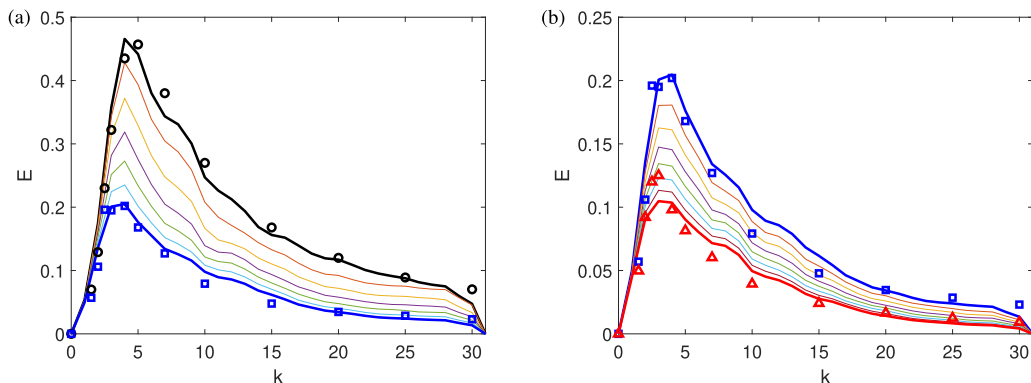


FIG. 7. Time evolution of energy spectra in a LES run (a) for time interval $U_0t/M = [42, 98]$, continuing in (b) for time interval $U_0t/M = [98, 171]$.

to properly capture the dissipation, attempts at DNS with such a resolution are expected to fail. In Fig. 6(b) we show the time evolution between the first and the last experimental station obtained in such underresolved DNS (also known as no-model LES). Because of a lack of sufficient dissipation at higher wave numbers, the kinetic energy tends to accumulate near the cutoff. The accompanying trend is increased energy transfer from the low-wave-number range, tilting the energy spectrum in an unphysical way.

The time evolution of the energy spectra in LES obtained using the present modeling procedure is shown in Fig. 7 and a number of turbulence parameters obtained in LES are compared with the experimental results in Table III. The comparison between LES and experimental parameters for two later times in the table is very good. There are discrepancies at the initial time, partly because the LES results are shown for a somewhat later time than $U_0t/M = 42$, namely, $U_0t/M = 51$, corresponding to the first thin line after the thick black line indicating the initial condition in Fig. 7(a). This was done to allow the nonlinear interactions to build up to develop correct kinetic energy decay which is needed to estimate the dissipation rate ε in LES through the kinetic energy decay rate $\partial\mathcal{E}/\partial t$. This quantity shows the largest discrepancy between LES and experiments, which is best explained using the classical estimate of the energy decay rate (equal to the dissipation rate) $du'^2/dt \sim u'^3/L_{\text{int}}$. Because of third power in u' , relatively benign differences in that quantity translate into larger differences for ε . These differences are due to the fact that the kinetic energy captured in the LES initial condition is necessarily lower than the experimental value, especially at earlier time (see Fig. 6). However, the experimental data and the numerical data in the first row for ε are self-consistent in the sense that $u'^3/L_{\text{int}} = 21.1$ and 45.6 for the numerical data and the experimental data, respectively, values which are relatively close to the corresponding values in Table III. This indicates that in both cases ε is appropriate for the initial spectra, the full experimental spectrum, and the truncated LES spectrum in Fig. 6. Most importantly, however, the time evolution of the energy spectrum is predicted quite well for the first time interval $U_0t/M = [42, 98]$. For the second time interval $U_0t/M = [98, 171]$ the energy peak is somewhat underpredicted at the final instant but the remainder of the LES curve matches experimental spectra accurately. Overall, these results demonstrate convincingly that the proposed method is capable of predicting the time evolution of turbulence for this classical case.

V. CONCLUSION

A previously proposed subgrid-scale modeling procedure [13], based on the interscale energy transfer among resolved scales in LESs, has been improved by increasing its reliance on information available directly from known LES fields. The procedure consists of two steps. In the first step,

the total unknown SGS transfer across a fixed cutoff wave number k_c is determined using the computed SGS transfer within the resolved range for the cutoff $\frac{1}{2}k_c$. In the second step a distribution of SGS transfer among resolved wave numbers $k < k_c$ is determined through an eddy viscosity shape function $f(k|k_c)$, normalized to unity at the cutoff k_c . The first step remains unchanged from the original method in [13] and its outcome is a ratio b of the SGS transfer at k_c due to scales below the test cutoff $\frac{1}{2}k_c$. The main change is how the shape function is determined. Originally, the prescribed functional forms of shape functions, suggested by the classical theories of turbulence, were considered. Such prescribed functions, characterized by a low-wave-number plateau and a cusp at the cutoff wave number k_c , were able to produce energy spectra in good agreement with the inertial range form when implemented in LESs. In this work the cusp's functional form was not prescribed but obtained directly from a k -dependent eddy viscosity computed using the actual resolved SGS transfer at the test cutoff $\frac{1}{2}k_c$. Such a computed eddy viscosity displays also a low-wave-number plateau but its value is too small because the resolved SGS transfer is lacking contributions from the nonlocal interactions with modes $k > k_c$. The missing interactions are accounted for by replacing the computed plateau by a constant value p , representing a constant asymptotic eddy viscosity acting on large eddies by small eddies in the presence of a spectral gap (here between $\frac{1}{2}k_c$ and k_c). For such a hybrid shape function the cusp is attributable to primarily local interactions and its values, greater than the plateau value p , are responsible for about 50% of the total SGS dissipation. This local transfer is not modeled but is a result of the actual interscale interactions operating at a given time step in actual LESs.

Tests of the original method were limited to LESs of forced high-Reynolds-number turbulence because the theoretical background behind the model development relied heavily on the inertial range dynamics. The procedure, as modified in this work, has been tested also in similar LESs of forced high-Reynolds-number turbulence and it was extended to decaying turbulence at both high and low Reynolds numbers. For high Reynolds number forced and decaying turbulence results met all expectations. The initial $k^{-5/3}$ spectrum is maintained correctly in LESs and the pulse-type initial condition evolves to the Kolmogorov form, in both cases with predicted values of the Kolmogorov constant in a generally accepted range, outside the forcing band. When forcing was removed for both initial conditions, energy spectra tended to the asymptotic Kolmogorov spectral form for wave numbers $k/k_c > 0.27$, with correct values of the Kolmogorov constant, while the total energy decayed by an order of the magnitude. Analyses of DNS results at low Reynolds numbers suggested that the constants b and p may be affected by the viscous effects and thus may not be universal. Nevertheless, when the method with both constants unchanged was used in LESs of the classical Comte-Bellot–Corrsin experiments the agreement between LES and experimental results was very good. Inspection of the experimental data shows that the LES wave-number cutoff is below the dissipation peak. This suggests that the method is not strictly dependent on details of the inertial range dynamics but rather that it may be sufficient for the dynamics to be only approximately inviscid. However, it is quite likely that the method will require modified constants for cutoffs in the dissipation range, but this is not a very important issue since for such situations DNSs are entirely feasible and one can dispense with LES entirely.

One of the secondary motivations behind this research is to explore what is minimum information input into LES as compared with DNS for the same physical problem. In the Introduction we postulated a target of fully autonomous LES, defined as a simulation that produces the same quality results within resolved range of scales as DNS and uses only the same information that is available to DNS. In the present paper we showed that information about the total SGS transfer and the partial dependence of the spectral eddy viscosity on k can be extracted from evolving LES fields, thus moving us in the direction of autonomous LES. At present the method requires constants b and p . Their values are determined from the asymptotics of the inertial range dynamics and are fixed for all flows considered in this work, but while required in LES, they are not needed in DNS of the same flows. We leave for future investigation whether information about constants b and p is possibly encoded in the resolved LES fields and how to extract it to make the method independent of any extraneous information input.

- [1] S. Toosi and J. Larsson, Anisotropic grid-adaptation in large eddy simulations, [Comput. Fluids](#) **156**, 146 (2017).
- [2] *Large Eddy Simulation of Complex Engineering and Geophysical Flows*, edited by B. Galperin and S. A. Orszag (Cambridge University Press, Cambridge, 1993).
- [3] M. Lesieur and O. Metais, New trends in large-eddy simulations of turbulence, [Annu. Rev. Fluid Mech.](#) **28**, 45 (1996).
- [4] U. Piomelli, Large-eddy simulations: Achievements and challenges, [Prog. Aerosp. Sci.](#) **35**, 335 (1999).
- [5] C. Meneveau and J. Katz, Scale-invariance and turbulence models for large eddy simulations, [Annu. Rev. Fluid Mech.](#) **32**, 1 (2000).
- [6] S. Pope, *Turbulent Flows* (Cambridge University Press, Cambridge, 2000).
- [7] J. A. Domaradzki and N. A. Adams, Direct modelling of subgrid scales of turbulence in large eddy simulations, [J. Turbul.](#) **3**, N24 (2002).
- [8] M. Lesieur, O. Metais, and P. Comte, *Large Eddy Simulations of Turbulence* (Cambridge University Press, Cambridge, 2005).
- [9] P. Sagaut, *Large-Eddy Simulation for Incompressible Flows*, 2nd ed. (Springer, Berlin, 2002).
- [10] R. Kraichnan, Eddy viscosity in two and three dimensions, [J. Atmos. Sci.](#) **33**, 1521 (1976).
- [11] J. Chollet and M. Lesieur, Parameterization of small scales of three-dimensional isotropic turbulence utilizing spectral closures, [J. Atmos. Sci.](#) **38**, 2767 (1981).
- [12] M. Lesieur, *Turbulence in Fluids*, 3rd ed. (Kluwer Academic, Dordrecht, 1997).
- [13] J. A. Domaradzki, Large eddy simulations of high Reynolds number turbulence based on interscale energy transfer among resolved scales, [Phys. Rev. Fluids](#) **6**, 044609 (2021).
- [14] J. Domaradzki and R. Rogallo, Local energy transfer and nonlocal interactions in homogeneous, isotropic turbulence, [Phys. Fluids A](#) **2**, 413 (1990).
- [15] J. A. Domaradzki and D. Carati, An analysis of the energy transfer and the locality of nonlinear interactions in turbulence, [Phys. Fluids](#) **19**, 085112 (2007).
- [16] Y. Zhou, Turbulence theories and statistical closure approaches, [Phys. Rep.](#) **935**, 1 (2021).
- [17] R. Rogallo, National Aeronautics and Space Administration Report No. 81315, 1981 (unpublished).
- [18] P. Yeung and S. Pope, An algorithm for tracking fluid particles in numerical simulations of homogeneous turbulence, [J. Comput. Phys.](#) **79**, 373 (1988).
- [19] N. P. Sullivan, S. Mahalingam, and R. M. Kerr, Deterministic forcing of homogeneous, isotropic turbulence, [Phys. Fluids](#) **6**, 1612 (1994).
- [20] R. Kraichnan, The structure of isotropic turbulence at very high Reynolds numbers, [J. Fluid Mech.](#) **5**, 497 (1959).
- [21] R. Kraichnan, Inertial-range transfer in two- and three-dimensional turbulence, [J. Fluid Mech.](#) **47**, 525 (1971).
- [22] J. Domaradzki and D. Carati, A comparison of spectral sharp and smooth filters in analysis of nonlinear interactions and energy transfer in turbulence, [Phys. Fluids](#) **19**, 085111 (2007).
- [23] J. Chollet, in *Turbulent Shear Flows 4*, edited by L. J. S. Bradbury, F. Durst, B. E. Launder, F. W. Schmidt, and J. H. Whitelaw (Springer, Berlin, 1984), pp. 62–72.
- [24] K. R. Sreenivasan, On the universality of the Kolmogorov constant, [Phys. Fluids](#) **7**, 2778 (1995).
- [25] R. Kerr, Velocity, scalar and transfer spectra in numerical turbulence, [J. Fluid Mech.](#) **211**, 309 (1990).
- [26] J. Domaradzki, Analysis of energy transfer in direct numerical simulations of isotropic turbulence, [Phys. Fluids](#) **31**, 2747 (1988).
- [27] J. A. Domaradzki, B. Teaca, and D. Carati, Locality properties of the energy flux in turbulence, [Phys. Fluids](#) **21**, 025106 (2009).
- [28] J. A. Domaradzki, R. Metcalfe, R. Rogallo, and J. Riley, Analysis of Subgrid-Scale Eddy Viscosity with Use of Results from Direct Numerical Simulations, [Phys. Rev. Lett.](#) **58**, 547 (1987).
- [29] J. A. Domaradzki, Nonlocal triad interactions and the dissipation range of isotropic turbulence, [Phys. Fluids A](#) **4**, 2037 (1992).
- [30] G. Comte-Bellot and S. Corrsin, Simple Eulerian time correlation of full-and narrow-band velocity signals in grid-generated, ‘isotropic’ turbulence, [J. Fluid Mech.](#) **48**, 273 (1971).